HHS Public Access

Author manuscript

Clin Cancer Res. Author manuscript; available in PMC 2019 July 15.

Published in final edited form as:

Clin Cancer Res. 2018 July 15; 24(14): 3409–3422. doi:10.1158/1078-0432.CCR-17-1717.

Combinatorial effects of VEGFR kinase inhibitor axitinib and oncolytic virotherapy in mouse and human glioblastoma stem-like cell models

Dipongkor Saha[1,2], **Hiroaki Wakimoto**[1,2], **Cole Peters**[1,2], **Slawomir J. Antoszczyk**[1,2], **Samuel D. Rabkin**[1,2], and **Robert L. Martuza**[1,2,*]

[1]Molecular Neurosurgery Laboratory and the Brain Tumor Research Center, Department of Neurosurgery, Massachusetts General Hospital, Boston, MA

[2]Department of Neurosurgery, Harvard Medical School, Boston, MA

Abstract

Purpose—Glioblastoma (GBM), a fatal brain cancer, contains a subpopulation of GBM stem-like cells (GSCs) that contribute to resistance to current therapy. Angiogenesis also plays a key role in GBM progression. Therefore, we developed a strategy to target the complex GBM microenvironment, including GSCs and tumor vasculature.

Experimental design—We evaluated the cytotoxic effects of VEFGR tyrosine kinase inhibitor (TKI) axitinib *in vitro* and then tested anti-tumor efficacy of axitinib in combination with oncolytic herpes simplex virus (oHSV) expressing anti-angiogenic cytokine murine IL12 (G47Δ-mIL12) in two orthotopic GSC-derived GBM models: patient-derived recurrent MGG123 GSCs, forming vascular xenografts in immune-deficient mice, and mouse 005 GSCs, forming syngeneic tumors in immune-competent mice.

Results—GSCs form endothelial-like tubes and were sensitive to axitinib. G47Δ-mIL12 significantly improved survival, as did axitinib, while dual combinations further extended survival significantly compared to single therapies alone in both models. In MGG123 tumors, axitinib was effective only at high doses (50 mg/kg), alone and in combination with G47Δ-mIL12, and this was associated with greatly decreased vascularity, increased macrophage infiltration, extensive tumor necrosis and PDGFR/ERK pathway inhibition. In the mouse 005 model, anti-glioma activity, after single and combination therapy, was only observed in immune-competent mice and not T cell-deficient athymic mice. Interestingly, immune checkpoint inhibition did not improve efficacy.

Conclusions—Systemic TKI (axitinib) beneficially combines with G47Δ-mIL12 to enhance anti-tumor efficacy in both immune-deficient and immune-competent orthotopic GBM models. Our results support further investigation of TKIs in combination with oHSV for GBM treatment.

[*]Corresponding Author: Robert L. Martuza, Mailing address: 185 Cambridge Street, CPZN-3800, Room 3816, Boston, MA 02114, Tel. 617.726-0339, Fax: 617.643-3422, rmartuza@mgh.harvard.edu.

Disclosure of Potential Conflicts of Interest: Samuel D. Rabkin and Robert L. Martuza are inventors on patents relating to oHSV owned by Georgetown University and Massachusetts General Hospital that have been licensed to Amgen, for which they receive royalties. The other authors declare no potential conflicts of interest.

Keywords

herpes simplex virus; cancer stem cells; anti-angiogenesis; glioma

INTRODUCTION

Glioblastoma (GBM) is the most common primary malignant brain tumor with no curative treatments (1). Despite advances in molecular understanding, diagnosis, and standard of care (surgical resection, radiation therapy and chemotherapy), overall median survival of GBM patients has only been extended to about 14 months (1). GBM stem-like cells (GSCs) isolated from GBM patient specimens have characteristics of self-renewal, differentiation into multiple mature lineages, and efficient tumorigenesis in immunodeficient mice that recapitulates the patient's tumor (2,3). Current conventional therapies typically fail to eradicate tumors and their GSCs, resulting in treatment-resistant recurrences (4,5). Angiogenesis also plays a key role in GBM progression (6–9) and anti-angiogenic therapy has been used for GBM treatment (10,11). However, Bevacizumab (Avastin®), an FDA approved anti-angiogenic drug (anti-VEGF), did not show significant improvement in overall survival in GBM patients (11,12). Therefore, other anti-angiogenic agents and combinatorial strategies are needed to target the complex GBM microenvironment, including GSCs and tumor vasculature.

GBM patients may be immune-competent or, more commonly, immune-suppressed by virtue of tumor burden as well as treatment with corticosteroids and chemotherapy. In order to study targeting of GSCs, tumor vascularity, and immunity, we studied both mouse (005) and human (MGG123) GSCs in immune-competent and -deficient mice. MGG123 GSCs were isolated from a recurrent human GBM patient and efficiently produce orthotopic tumors in athymic nude mice (13). The tumors are invasive, morphologically heterogeneous, and hypoxic with abnormal vasculature, similar to what occurs in human GBM (13). Recently, our laboratory also described an immune-competent GBM model derived from mouse 005 GSCs, which form intracranial tumors in syngeneic C57BL/6 mice (14). 005 GSCs were isolated from gliomas arising after lentiviral transduction of brains with activated Harvey-Ras (H-Ras) and protein kinase B (Akt), in tumor suppressor gene p53 $(Tp53)^{+/-}$ mice (15). They are highly tumorigenic in syngeneic mice and their tumors are histologically similar to human GBM, demonstrating tumor heterogeneity, immune-suppression, invasiveness, and high vascularity (14). Thus, both MGG123 and 005 GSC models provide a platform to study targeting the complex tumor microenvironment, including GSCs and tumor vascularity, in both an immune-deficient and immune-competent state.

Oncolytic virotherapy is a therapeutic strategy that utilizes the selective replication and cytotoxicity of viruses towards cancer, including GBM (16,17). Oncolytic herpes simplex virus (oHSV) is genetically engineered to specifically replicate in and kill cancer cells, while sparing normal cells (18). During this process, oHSV is amplified, spreads through the tumor, and induces anti-tumor immune responses (19). The FDA recently approved the first oncolytic virus, an oHSV expressing GMCSF (talimogene laherparevec, T-Vec), for the

treatment of metastatic melanoma, which has shown promising efficacy with tolerable side effects (20). T-Vec has not yet been demonstrated to be safe following intracranial injection. For these studies, we use G47Δ as our base oHSV, which is similar to T-Vec without GMCSF (21), and has been shown to be safe following intracranial injection (22), and is currently in clinical trial for recurrent GBM in Japan (WHO JPRN-UMIN000002661). To improve the anti-tumor efficacy of G47Δ, we have inserted the anti-angiogenic cytokine IL-12 (G47Δ-mIL12) (14,23). IL12 expression enhances the activity of G47Δ in human and mouse GBM models (14,23). In immune-deficient models, observed anti-tumor efficacy of G47Δ-mIL12 is mainly due to the significant inhibition of neovascularization, whereas in immune-competent models, anti-tumor effects of G47Δ-mIL12 are largely T cell dependent (14,23). We hypothesized that the combination with other therapeutic strategies will improve therapeutic outcomes from G47Δ-mIL12.

Axitinib (AG-013736) is an orally administered potent small molecule tyrosine kinase inhibitor (TKI), which inhibits VEGFR-1, -2 and -3, as well as PDGFRb and c-KIT (CD117) (24). It has been approved for use in advanced renal cell carcinoma, where it was superior to sorafenib (Nexavar) (25) and shows promising antitumor activity in a variety of other advanced cancers, including GBM (26–29). We previously showed that axitinib produced modest anti-tumor efficacy in both patient GSC-derived xenografts and mouse 005 GSC-derived syngeneic models, which was associated with significant inhibition of neovascularization and induction of apoptosis (30). Axinitib also induces anti-tumor immune effects, including increased tumor infiltration of immune effector cells (31,32). Therefore, it was reasonable to test the combination of axitinib with oHSV.

In this study, we first examined the effect of axitinib on GSCs *in vitro* and then synergy with G47Δ-mIL12 in inhibiting GBM growth in a human recurrent GSC-derived GBM model in athymic mice. This was then compared to the immune-mediated effects of combinatorial axitinib plus G47Δ-mIL12 therapy in a mouse syngeneic GSC derived GBM model. In both models, the combination improved survival.

MATERIALS AND METHODS

Cells, Virus and drug

GFP-positive mouse 005 GSCs (15,33) were cultured as spheres in serum-free stem cell medium composed of advanced DMEM/F12 medium (ThermoFisher Scientific), supplemented with 2 mM L-glutamine (Corning), 1% N2 supplement (ThermoFisher Scientific), 2 μg/mL heparin (Sigma-Aldrich), 0.5% penicillin G-streptomycin sulfate-amphotericin B complex (Corning), recombinant human EGF (20 ng/mL; R&D systems), and recombinant human FGF-basic (20 ng/ml; Peprotech) (14). Neurospheres were dissociated with Accutase (Innovative Cell Technologies) for passaging. Mouse brain microvascular endothelial cells (MBMECs) were obtained from Cell Biologics and cultured in mouse endothelial cell medium supplemented with 0.1% vascular endothelial growth factor, 0.1% endothelial cell growth supplement, 0.1% heparin, 0.1% EGF, 0.1% hydrocortisone, 1% L-glutamine, 1% antibiotic-antimycotic solution, and 5% fetal bovine serum (Cell Biologics). MBMECs were trypsinized with 0.25% trypsin supplemented with 0.53 mM EDTA (Corning) for passaging. Human primary (MGG4, MGG8, MGG23, and

MGG64) and recurrent GSCs (MGG31, MGG50, MGG85, MGG91, and MGG123) were described previously or isolated from discarded GBM specimens (3,13,34). Human GSCs were cultured as spheres in EF20 stem cell medium composed of neurobasal medium (ThermoFisher Scientific), supplemented with 3 mM L-glutamine (Corning), 1% B27 supplement (ThermoFisher Scientific), 0.5% N2 supplement (ThermoFisher Scientific), 2 μg/mL heparin (Sigma-Aldrich), 0.5% penicillin G-streptomycin sulfate-amphotericin B complex (Corning), recombinant human EGF (20 ng/mL; R&D systems), and recombinant human FGF-basic (20 ng/ml; Peprotech). GSCs were dissociated with Accutase or NeuroCult™ Enzyme Dissociation Kit (Stemcell Technologies). Cells were low-passage and confirmed to be mycoplasma-free (LookOut mycoplasma kit; Sigma).

G47Δ-mIL12 was constructed from G47Δ (deletions in γ34.5 and α47 genes and inactivating insertion of LacZ into ICP6 (21)) by insertion of mouse IL-12 cDNA (p35 and p40 separated by bovine elastin motifs) into the ICP6 gene (14). Axitinib (AG-013736; kindly provided by Pfizer) was dissolved in DMSO and a 25 mM stock solution was prepared for *in vitro* studies. The highest DMSO concentration (0.4% DMSO) used for *in vitro* studies was non-toxic to the cells.

Cytotoxicity assays

Dissociated (mouse 005 GSCs and human GSCs) or trypsinized (MBMECs) cells were seeded into 96-well cell culture plates (3000 mouse GSCs, 8000 human GSCs, or 500 MBMECs/well). Axitinib was added to cells immediately after seeding and incubated for 4 (005 GSCs), 5 (MBMEC), or 6 days (human GSCs) at 37°C before MTS assays were performed following manufacturer's instruction (Promega). G47Δ-mIL12, diluted in 'no heparin' medium, was added to the cells immediately (MBMECs), or 6–24 hrs (005 GSCs) after seeding and incubated at 37°C. Two hr post-virus infection, medium 'with heparin' was added, and 4 (005 GSCs) or 5 days (MBMEC) post-seeding, MTS assays were performed. Each experiment was repeated at least two independent times and performed in triplicate. Dose-response curves and IC50 values were calculated using Prism 7 GraphPad software version 7.0a.

Tube formation assay

Mouse 005 GSCs (8×10^4/well), human GSCs ($8–10 \times 10^4$/well), or MBMECs (4×10^4/well) were resuspended in 1 ml EGM-2 (Lonza; for mouse and human GSCs) or mouse endothelial cell medium (for MBMECs) with or without axitinib, plated into 24-well cell culture plates pre-coated with 250 μl of Matrigel (BD Bioscience) and incubated at 37°C. 15–30 (human GSCs) or 19 (005 cells) hr later, microscopic pictures were captured and tube formation was assessed by counting the tube branching points.

Flow Cytometry

GSCs were grown in endothelial cell growth medium (EGM)-2 supplemented with the bullet kit (Lonza) for 3 days at 37°C. Cells were dissociated, spun, counted, re-suspended in FACS buffer (2% inactivated fetal calf serum in PBS), incubated with FITC-conjugated anti-human CD31 (Biolegend) for 30 min at room temperature, washed, fixed in 4% paraformaldehyde,

washed, re-suspended in 2% FACS buffer and sorted by LSRII flow cytometer (BD Biosciences). Data were analyzed with FlowJo software v.10.1 (Tree Star).

Secondary neurosphere formation assay and in vitro limiting dilution studies

Single cell suspensions of 005 GSCs were either pre-treated with axitinib and/or G47Δ-mIL12 before clonogenic plating into 96-well plates at 10 or 30 cells/well free of therapies, or continuously exposed to non-toxic concentration of axitinib and/or G47Δ-mIL12. After 12 days of incubation, average number of spheres/well was recorded.

For *in vitro* limiting dilution study, 005 cells (0.5, 1, 2, 3, 4, 8, 10, 16, or 32 cells/well) were plated in 96-well plate. Cells were continuously exposed to a non-toxic concentration of axitinib and/or G47Δ-mIL12 for 12 days and the number of wells containing spheres were recorded and plotted using ELDA: Extreme Limiting Dilution Analysis form, as described (35). Treatment groups were compared to each other using a Chi Square test.

Mouse studies

C57BL/6 or athymic mice (7–8 weeks old) were obtained from the National Cancer Institute (Frederick, MD). All mouse procedures were approved by the Institutional Animal Care and Use Committee at the Massachusetts General Hospital. Dissociated 005 GSCs (2×10^4 cells) or MGG123 GSCs (5×10^3 cells) in 3 μl of their respective media were implanted stereotaxically into the striatum (2.2-mm lateral from Bregma and 2.5-mm deep) to generate orthotopic intracranial tumors. On indicated days after tumor implantation, mice were randomly divided into groups, intratumorally injected once or twice with G47Δ-mIL12 (as indicated) or PBS in 2 μl at the same stereotaxic coordinates, and/or injected intraperitoneally with axitinib (25 or 50 mg/kg; dissolved in polyethylene glycol 400 and acidified water, pH adjusted to 2.5–3) or vehicle solution for 1–3 cycles (1 cycle = 5 days on and 2 days off). Immune checkpoint inhibitor anti-mCTLA-4 antibodies (Syrian hamster clone 9H10; 5 mg/kg) or isotype control antibodies (Syrian hamster IgG) were obtained from BioXcell and administered 3-times intraperitoneally on indicated days after tumor implantation. Mice were followed for neurological symptoms and euthanized before becoming moribund. Animal caretakers were blinded to the treatment. Presence of tumor at sacrifice was evaluated macroscopically or after histological staining of sections.

Immunohistochemistry

Mouse brains were removed, fixed in 10% formalin, embedded in paraffin, and 5 μm sections subjected to immunohistochemistry (IHC) and standard hematoxylin and eosin (H & E) staining. Formalin-fixed paraffin-embedded (FFPE) sections were treated with xylene, followed by gradual rehydration in 100%, 90% and 70% ethanol, then in distilled water. Rehydrated sections were then subjected to heat-mediated antigen retrieval using 10 mM sodium citrate buffer, washed in PBS, incubated with Bloxall™ blocking solution (Vector Lab; to block endogenous peroxidase activity), washed in PBS, incubated with 5% bovine serum albumin, followed by 5% goat or horse serum, and then incubated overnight at 4°C with rat anti-mouse CD34 (1:150; abcam, cat. # ab8158), rabbit anti-mouse Ki67 (1:100; abcam, cat. # ab16667), rabbit anti-mouse CD3 (1:100, abcam, cat. # ab5690), rat anti-mouse CD4 (1:200, eBioscience, cat. # 14-9766-80), rat anti-mouse CD8a (1:100,

eBioscience, cat. # 14-0808-80), rabbit anti-FoxP3 (1:500, abcam, cat. # ab54501), rabbit anti-CD68 (1:400, abcam, cat. # ab125212), rabbit anti-Granzyme B (1:150, abcam, cat. # ab4059), rabbit anti-cleaved caspase-3 (1:100, Cell Signaling, cat. # 9661), rabbit anti-SOX2 (1:1000, abcam, cat. # ab97959), or rabbit anti-NeuN (1:400, Cell signaling, cat. # 24307). Following 3 washes in PBS, sections were incubated with HRP-conjugated anti-rat Ig, or HRP-conjugated anti-rabbit Ig for 30 minutes at room temperature, followed by 3 × PBS wash and DAB staining (DAKO). Sections were counterstained with hematoxylin, dehydrated, and mounted in CYTOSEAL™ XYL (Thermo Scientific). Cell counts were from at least 3–5 random fields / tumor section (n=3 or 4 mice/group) as indicated. ImageJ software (NIH) and ImageQuant by Molecular Dynamics software were used to quantify the $CD34^+$ areas and tumor volume, respectively. Counter was blinded to the treatment.

Signal transduction studies

For *in vitro* studies with HUVEC, MBMEC and MGG123, cells were starved (no growth factors) overnight, followed by stimulation with or without human or mouse VEGF (100 ng/ml; Sino Biological Inc.) or PDGF-BB (100 ng/ml; Peprotech) for 15 min. Simultaneously, cells were also treated with or without axitinib at indicated doses for 15 min. For combination treatment, MGG123 cells were treated with or without G47Δ-mIL12 (moi 1.0) and incubated 6 hr at 37°C. During the last 15 min of viral incubation, PDGF and vehicle or axitinib were added to the cells. Cells were then lysed in RIPA buffer (Boston Bioproducts) in the presence of protease/phosphatase inhibitors (Roche). 15–20 μg of cell lysates were then subjected to western blot, as described (36). Each experiment was repeated at least two times and the western blot data were quantified using Image Lab Software Version 5.1.

To evaluate the treatment effects of combination therapy (axitinib+G47Δ-mIL12) *in vivo* in MGG123 tumors, athymic mice were implanted with MGG123 GSCs on day 0, high-dose axitinib (50 mg/kg) or vehicle solution was injected intraperitoneally from days 13–17, and/or G47Δ-mIL12 (5×10^4 pfu) or PBS injected intratumorally on day 15. 3 hr after the last axitinib injection (i.e., day 17), mice were sacrificed (3–4 mice/group) and brain tumor lysates were subjected to western blot analysis.

Statistical analysis

One-way ANOVA followed by Tukey's multiple comparison test was used to compare the different treatment groups in the tube formation assay experiment. Survival data were analyzed by Kaplan Meier survival curves, and comparisons were performed by Log Rank test. Immunohistochemistry counts were compared using an unpaired two-tailed Student *t* test. *P* values of less than 0.05 were considered significant. All statistical analyses were performed using Prism 7 GraphPad software version 7.0a.

RESULTS

Sensitivity of GSCs and MBMECs to axitinib and G47Δ-mIL12 in vitro

We first tested the sensitivity of mouse 005 GSCs and MBMECs to axitinib and G47Δ-mIL12. Both 005 GSCs and MBMECs were sensitive to axitinib with IC50s of 1 and 2 μM,

respectively (Fig. 1A). 005 GSCs were sensitive to G47Δ-mIL12 (IC50 = MOI 0.7), while MBMECs were resistant (Fig. 1B). Heparin, added to the medium to increase the stability of fibroblast growth factor (FGF) (37), blocked virus sensitivity (Supplementary Fig. S1A, B) (38) so it was absent during oHSV infection. Mouse 005 GSCs form tubes *in vitro* when grown in endothelial cell growth media (EGM-2). 005 tube formation *in vitro* was inhibited 45% by 0.03 μM axitinib (Fig. 1C, D, $p < 0.0001$), while MBMEC tube formation was not sensitive to axitinib, up to 3 μM.

We previously showed that human primary GSCs were sensitive to axitinib (30). Here we tested the sensitivity of human recurrent GSCs; MGG50 and MGG123 GSCs were sensitive to axitinib, with IC50s of ~1.2 μM and ~2.5 μM, respectively, while MGG85 was resistant (Fig. 1E). None of the primary GSCs formed tubes *in vitro*, except MGG64, which showed a trend of tube formation (Supplementary Fig. S1C), whereas of five recurrent GSC lines tested, MGG50, MGG85, and MGG123 formed tubes (Supplementary Fig. S1D; upper panel) and MGG31 and MGG91 showed a trend of tube formation in matrigel-based media (Supplementary Fig. S1D; lower panel). None of the primary and recurrent GSCs expressed CD31 (Supplementary Fig. S1E, F). Tubes derived from MGG50, MGG85 and MGG123 were not sensitive to axitinib up to 10 μM (Supplementary Fig. S1G).

Depletion of stem-like population by individual or combination therapy (axitinib+G47Δ-mIL12)

In previous studies, it was reported that axitinib (30) or oHSV G47Δ treatment alone (34) inhibits secondary neurosphere formation, a hallmark of stem-like properties. We determined the effects of the combination therapy (axitinib+G47Δ-mIL12) on the ability of 005 GSCs to form clonogenic spheres. Cells were either pre-treated with axitinib (10 uM) and/or G47Δ-mIL12 (moi 0.2) before clonogenic plating free of therapies (Supplementary Fig. S2A), or continuously exposed to non-toxic concentration of axitinib (300 nM) and/or G47Δ-mIL12 (moi 0.2) for 12 days (Supplementary Fig. S2B). In both experiments, single treatments were significantly effective in reducing neurosphere formation compared to mock treatment ($p<0.05$), and the combination treatment was even significantly better than either single treatment alone ($p<0.05$), indicative of effective depletion of the stem-like population (Supplementary Fig. S2A, B). *In vitro* limiting dilution assays also showed that the proportion of stem-like cells was significantly decreased after combination therapy compared to single treatments (Fig. 1F).

Efficacy of combination therapy (axitinib+G47Δ-mIL12) in an orthotopic angiogenic human GSC-derived GBM model

In previous studies we demonstrated that: (i) axitinib treatment alone produces only a modest prolongation in survival in orthotopic primary GSC-derived human glioma xenograft models that was associated with a large decrease in angiogenesis (30); and (ii) IL12 expression from G47Δ (G47Δ-mIL12 versus G47Δ-empty) reduced angiogenesis *in vivo* and extended survival of mice bearing MGG4 primary GSC-derived tumors (23). Therefore, we explored whether axitinib would improve the therapeutic efficacy of G47Δ-mIL12 *in vivo*. For these studies, we used axitinib-sensitive MGG123 recurrent GSCs, which form aggressive and highly vascular orthotopic tumors (13). Athymic mice bearing MGG123

GSC-derived brain tumors were treated with intraperitoneal injections of axitinib (25 mg/kg) or vehicle from days 12 to 16 once daily and with a single intratumoral injection of G47Δ-mIL12 or PBS on day 14 (Fig. 2A). G47Δ-mIL12 treatment alone significantly extended median survival (median survival=29 days) compared to mock (median survival= 22 days; p=0.0005), by 32% (Fig. 2A). No extension was seen with axitinib alone (p=0.16), although $CD34^+$ tumor vascularity was significantly reduced by axitinib treatment compared to mock (P=0.0006) (2B). This suggests that the axitinib dose and/or short treatment period were insufficient to control the growth of MGG123 GSC-derived tumors. The combination (median survival=27 days) was no different than virus alone (p=0.8; Fig. 2A).

To increase the effects of axitinib, we doubled the dosage (to 50 mg/kg) and continued treatment for 2 cycles, from days 5 to 16 (Fig. 2C). In this case, axitinib (median survival=30 days) or G47Δ-mIL12 (median survival=33 days) alone significantly extended median survival compared to mock treatment (median survival=26.5 days; p=0.009 and p=0.001, respectively) (Fig. 2C). Here, high-dose axitinib resulted in almost complete reduction of $CD34^+$ vascularity compared to mock (Fig. 2D; p<0.0001). Now, combination therapy (axitinib+G47Δ-mIL12; median survival=42.5 days) further prolonged survival compared to axitinib (p=<0.0001) or G47Δ-mIL12 (median survival=33 days; p=0.02) treatment alone, and resulted in 1 long-term survivor (Fig. 2C), which had no evidence of tumor (Fig. 2E).

Histopathology of treated human GBM

Next, we examined the effects of treatment on tumor histopathology. Athymic mice bearing MGG123 GSC-derived brain tumors were treated with high-dose axitinib (50 mg/kg) and/or G47Δ-mIL12 (as in Fig. 2C), and 24 hr after the last axitinib injection (i.e., day 17), mice were sacrificed and brains collected. Staining for CD34 (vascularity) illustrated the anti-angiogenic effects of axitinib treatment, either alone or in combination (Axi, Axi+V; Fig. 3A). Quantification revealed that high-dose axitinib treatment resulted in a 5.4-fold decrease in vascularity compared to mock (Fig. 3B; p<0.0001), which was 2.8-times larger than low-dose axitinib, which only had a 1.9-fold decrease in vascularity compared to mock (Fig. 2B, D). G47Δ-mIL12 treatment did not significantly alter vascularity compared to mock, while the combination was somewhat more vascular than axitinib alone (Fig. 3A, B). Axitinib treatment alone (p=<0.001) or in combination (p=<0.01) significantly enhanced infiltration of $CD68^+$ tumor-associated macrophages (TAMs) within the MGG123 tumors compared to mock or virus treatment alone (Fig. 3A, B). Similar to what we previously reported for U87 tumors (30), axitinib treatment reduced proliferating cells ($Ki67^+$) in the tumor (Fig. 3A, B) and cellular density, which was further reduced after combination treatment (Fig. 3C). Tumor size at this early time point was smaller in the axitinib-treated group compared to the mock and virus treated groups (Fig. 3D, E). The issue of hemorrhage has been a concern for treatment of brain tumors with the combination of anti-angiogenic compounds plus oncolytic virus. However, we found that this combination produced large necrotic areas throughout the tumor but no significant hemorrhage, indeed, less than is seen with virus alone (Fig. 3E, Supplementary Fig. S3A). No qualitative difference was observed in the $NeuN^+$ staining cells (neuronal marker) between any of the treatments groups (Supplementary Fig. S3B). Oncolytic virus treatment alone produced increased levels of

apoptosis (cleaved caspase 3) in the MGG123 GSC-derived tumors, compared to mock or axitinib treatment, which was further enhanced with combination treatment (Supplementary Fig. S4A). Sox2 expression (stem cell marker) was greatly reduced in tumors after combination therapy (Supplementary Fig. S4B), suggesting that combination treatment affected the stem-like population *in vivo*.

Combination therapy (axitinib+G47Δ-mIL12) blocks PDGFR/ERK pathway in MGG123 GBM model both in vitro and in vivo

Since axitinib is a multi-tyrosine kinase inhibitor, we performed signal transduction studies both *in vitro* and *in vivo*. First, we tested the effects of axitinib on VEGFR/PDGFR and their downstream ERK/AKT pathways in both human (HUVEC) and mouse (MBMEC) endothelial cells and MGG123 tumor cells. In HUVEC, axitinib (10 μM) blocked phosphorylation of both VEGFR2 (p-VEGFR2) and PDGFRβ (p-PDGFRβ) and downstream phospho-ERK1/2 (p-ERK1/2) and phospho-AKT (p-AKT) (Supplementary Fig. S5A). In MBMEC, which is more relevant in the context of brain tumor angiogenesis, axitnib (10 μM) treatment blocked both p-ERK1/2 and p-AKT (Supplementary Fig. S5B). MGG123 tumor cells express PDGFRβ, not VEGFR2 (Fig. 4A). Therefore, we examined the effects of axitinib and/or G47Δ-mIL12 in PDGFR pathway. p-PDGFRβ was completely blocked by axitinib treatment (10 μM) (Fig. 4A). Dose-dependent inhibition of p-PDGFRβ and its downstream p-ERK1/2 and p-AKT were also observed, with strong or complete inhibition observed at a dose of 1 μM (Fig. 4B, C). Based on the dose-dependent effects of axitinib on p-PDGFRβ, p-ERK1/2 and p-AKT (Fig. 4B, C), three different doses of axitinib (111, 333, and 1000 nM) were chosen to examine effects of combination (axitinib+G47Δ-mIL12) in PDGF-stimulated MGG123 cells. Axitinib alone (all three doses) or combination with virus reduced the levels of p-PDGFRβ by ~80–100%, compared to PDGF-stimulated cells (Fig. 4D, Supplementary Fig. S5C). Virus treatment alone decreased p-ERK1/2 expression by 15%, and axitinib reduced it by ~50% (axitinib 111 nM) to 83% (axitinib 1000 nM) (Fig. 4D, Supplementary Fig. S5C). Combination treatment was similar to axitinib treatment alone in inhibiting phosphorylation of ERK1/2 (Fig. 4D, Supplementary Fig. S5C). As expected, virus treatment enhanced p-AKT by 70%, as previously shown by Kanai et al (36), however, AKT activation was reduced to ~25% by axitinib treatment (333 nM or 1000 nM) (Fig. 4D, Supplementary Fig. S5C).

Since axitinib and combination therapy targeted the key downstream effector ERK1/2 in both GSCs and endothelial cells, we evaluated treatment effects on p-ERK1/2 in MGG123 tumor *in vivo*. Single treatments reduced p-ERK1/2 levels by 20%, compared to mock, and the combination therapy further reduced it by ~25%, compared to each single treatment alone (Fig. 4E, F).

Anti-tumor efficacy of G47Δ-mIL12 in immunocompetent mice was enhanced by axitinib therapy

Axitinib and G47Δ-mIL12 as single treatments have modest anti-tumor effects in immunocompetent 005 GSC-derived brain tumors (14,30), and the anti-tumor efficacy of G47Δ-mIL12 is largely T-cell mediated (14). Axitinib is reported to increase immune cell infiltration and reduce suppressive MDSCs in brain metastasis (31,32), but not to suppress

effector T cells, in contrast to other TKIs (39). Therefore, we hypothesized that combining axitinib with G47Δ-mIL12 would improve anti-tumor efficacy by targeting both immune and vasculature components of the tumor microenvironment. C57BL/6 mice bearing established 005 GSC-derived brain tumors were treated with two intratumoral injections of G47Δ-mIL12 or PBS on days 11 and 17 and intraperitoneal axitinib (25 mg/kg) or vehicle from days 14 to 32 (3 cycles of 5 days on and 2 days off) (Fig. 5A). Both axitinib (median survival=41 days) and G47Δ-mIL12 (median survival=37 days) modestly, but significantly, improved median survival compared to mock (median survival=33 days; p=0.0003 and p=0.03, respectively) (Fig. 5A). Combination therapy (axitinib+G47Δ-mIL12) further extended survival significantly compared to axitinib (p=0.04) or G47Δ-mIL12 (p=0.002) treatment alone, and resulted in 2 longer-term survivors (Fig. 5A), although both mice had large tumors (Supplementary Fig. S6A), so tumor growth was just slowed not eradicated. This suggests that extending the number of treatment cycles may be beneficial.

Immunohistochemistry for $CD3^+$ T cells was performed in the tumor and non-tumor areas in order to assess untoward inflammatory responses within the surrounding brain at the point of death (Supplementary Fig. S6B). A large presence of $CD3^+$ T cells was only observed in the tumor areas. Its limited presence in non-tumor areas in all treatment groups indicated no untoward inflammatory responses in the surrounding brain tissues (Supplementary Fig. S6B).

Anti-tumor effects of axitinib+G47Δ-mIL12 combination therapy in the 005 model was T-cell dependent

Because axitinib and G47Δ-mIL12 modulate immune cells in syngeneic tumor models (14,31), we tested whether the survival benefits of axitinib+G47Δ-mIL12 combination therapy in C57BL/6 mice were immune-mediated. Therefore, we next studied athymic mice (devoid of T cells) bearing intracranial 005 GSC-derived tumors and treated them with intratumoral injections of G47Δ-mIL12 or PBS on days 11 and 17 and intraperitoneal axitinib or vehicle from days 14 to 25 for 2 cycles (Fig. 5B). As opposed to the C57BL/6 immune-competent mice, there was no significant difference in median survival between the single or combination treatments compared with mock in athymic mice (Fig. 5B), indicating that the therapeutic efficacy of axitinib+G47Δ-mIL12 combination therapy in 005 mouse tumors was T-cell dependent.

Addition of immune checkpoint inhibitor did not improve the therapeutic outcome of axitinib+G47Δ-mIL12 combination therapy

Given the T cell dependency of axitinib+G47Δ-mIL12 anti-tumor efficacy, we asked whether combining this with immune checkpoint blockade would improve the outcome. We used anti-CTLA-4 antibodies for immune activation of T cells (40). C57BL/6 mice bearing 005 GSC-derived tumors were treated with triple combination therapy (axitinib+anti-CTLA-4+G47Δ-mIL12) using the treatment regimen shown in Fig. 5C. Anti-CTLA-4 alone had a significant but modest effect (versus Mock), similar to axitinib or G47Δ-mIL12 alone, but none of the combinations further extended survival (Fig. 5C), suggesting that checkpoint blockade might have antagonized the combination effect of axitinib with G47Δ-mIL12.

Treatment effects of axitinib+G47Δ-mIL12 combination therapy on immune cells and other cell markers in 005 GBM model

Finally, we used immunohistochemistry for immune cells and other cell markers to better understand the anti-tumor effects of axitinib+G47Δ-mIL12 combination therapy in the 005 model. C57BL/6 mice bearing 005 GSC-derived tumors were treated with intratumoral injections of G47Δ-mIL12 or PBS on days 18 and 24 and intraperitoneally with axitinib or vehicle from days 21 to 25. Six hours after the last axitinib injection, animals were sacrificed and brains collected. Axitinib treatment alone or in combination with virus reduced vascularity and $CD34^+$ cells, but not significantly compared to mock (Fig. 6A, B). Axitinib or combination treatment did not significantly alter (as opposed to mock treatment) the number of tumor infiltrating $CD68^+$ macrophages, Granzyme B^+ activated cytotoxic cells, $Ki67^+$ proliferating cells, $FoxP3^+$ cells, or cleaved caspase 3^+ apoptotic cells (Fig. 6A–D). In contrast to the axitinib-mediated effects on T cells previously reported (31,32), the number of $CD3^+$ ($p=0.003$) and $CD8^+$ ($p=0.03$) cells were reduced after axitinib treatment compared to mock (Fig. 6A, B). However, the combination with G47Δ-mIL12 overcame these negative effects, significantly increasing tumor infiltrating $CD3^+$ ($P=<0.001$) and $CD4^+$ ($P=0.002$) cells compared to axitinib alone (Fig. 6A, B).

Discussion

We show that TKI inhibitor axitinib combined with oHSV G47Δ-mIL12 enhanced survival of GSC-derived brain tumors. In the human hyper-vascular GSC-derived GBM model, anti-tumor efficacy of axitinib was dose-dependent, while in the syngeneic GSC model (005) it was T cell dependent. The interactions are complex and may be impacted by the temporal dosing regimen.

Both mouse 005 GSCs and MBMECs are highly sensitive to axitinib treatment. Recurrent MGG50 and MGG123 GSCs were sensitive to axitinib with IC50s of 1.2 and 2.5 μM, which is quite similar to that reported for primary GSC lines (30) and glioma cell lines (41), while MGG85 GSCs were relatively resistant. MBMECs were resistant to G47Δ-mIL12, as expected due to the non-permissivity of normal cells. Heparin present in medium can inhibit G47Δ-mIL12 infectivity and thus should be removed when testing oHSV *in vitro*. Human primary GSCs have already been shown to be sensitive to G47Δ virus (34,42).

An anti-angiogenic agent like axitinib has the potential to modulate the tumor microenvironment and improve immunotherapy, however, anti-angiogenic agent dosage is a determining factor in the therapeutic response (43). Axitinib treatment alone (administered @ 25mg/kg; low dose) caused significant but modest extension of survival in human orthotopic glioma (U87) and primary GSC-derived (MGG4) xenograft models, and was associated with a reduction of $CD34^+$ vascularity (30). In contrast, the same axitinib dose alone or in combination did not produce any effects on survival of mice with MGG123 tumors, even though $CD34^+$ vascularity was reduced. Doubling the axitinib dose (50 mg/kg; high dose) and treatment cycles (to two) produced much larger effects on $CD34^+$ vascularity and survival either alone or in combination with oncolytic G47Δ-mIL12 in the MGG123 model. IC50 of axitinib in MGG123 GSCs was 2.5 times higher than that in 005 GSCs, which might explain why high dose axitinib was necessary to have the combination effects

in vivo in the MGG123 model. Alternatively, potent anti-angiogenic effect of axitinib is important for combination effects with oHSV. The beneficial effects of axitinib dose escalation have also been reported in patients with progressive metastatic renal cell carcinoma, where axitinib dose escalation showed a decrease in tumor burden in a large proportion of patients (78%) (44). These dose-dependent effects of axitinib were in contrast to what was seen in immune-competent models. For example, lower doses of anti-VEGFR2 antibody produced superior anti-tumor effects than higher doses, and enhanced efficacy of vaccine therapy in immune-competent breast cancer models (43). These low dose anti-VEGFR2-mediated anti-cancer effects were associated with the normalization of the breast tumor vasculature, not anti-angiogenesis (43). In the immune-competent 005 GSC model, low-dose axitinib in combination with G47Δ-mIL12 was sufficient in controlling tumor growth without producing significant anti-angiogenic effects, an effect that was T-cell dependent.

Treatment with TKIs, such as axitinib, has been shown to enhance T cell infiltration within the tumor microenvironment in an intracranial melanoma model (31), which is different from our findings where axtinib treatment significantly reduced $CD3^+$ and $CD8^+$ T cell infiltration in orthotopic 005 tumors. It is not clear how axitinib negatively regulated T cell infiltration in the 005 tumors. Several TKIs (ie., sunitinib, sorafenib, and axitinib) were shown to suppress T cell proliferation *in vitro* (39). Cabozantinib, a TKI similar to axitinib, reduces tumor cell proliferation and vascularity, and enhances T cell mediated killing of tumor cells (45). Although TKI therapy alone may be beneficial or detrimental to T cell responses, combining TKI with cancer vaccines can be beneficial in inducing T cell mediated anti-tumor responses (45,46). For example, when cabozantinib was given in combination with a poxvirus based therapeutic cancer vaccine (45) or axitinib in combination with an adenoviral based vaccine producing IL-12 (46), a significant T cell dependent synergy was observed in controlling tumor growth, and an anti-VEGFR2 antibody+cancer vaccine combination had T cell dependent anti-cancer effects in breast cancer models (43). In the 005 GBM model, axitinib-mediated anti-tumor effects are mainly T cell dependent, as also seen in (45), without significantly affecting tumor vascularity. Similar to anti-VEGFR2+cancer vaccine combination therapy, the anti-glioma effects of our combination treatment (axitinib+G47Δ-mIL12) were also T cell dependent.

Anti-angiogenic therapy can beneficially impact immunotherapy (47). Because axitinib +G47Δ-mIL12 combination therapy of 005 tumors involves T cells, we sought to study whether anti-tumor efficacy could be improved by adding immune checkpoint blockade immunotherapy, such as anti-mCTLA-4. However, anti-mCTLA-4 was not efficacious in enhancing the anti-tumor effects of axitinib+G47Δ-mIL12, and was potentially counterproductive. In previous studies combining G47Δ-mIL12 with checkpoint blockade, inhibiting the PD-1/PD-L1 pathway resulted in similar survival extension as anti-CTLA-4 (33), so we do not anticipate a difference when anti-PD-1 is combined with axitinib and G47Δ-mIL12. We speculate that decreased vascular permeability due to axitinib treatment (48) inhibited extravasation of T cells to the tumor. There was a significant decrease in $CD3^+$ and $CD8^+$ T cell infiltration in the tumor after axitinib treatment, although this was overcome by virus. In recent studies with an intracranial B16 melanoma model, a small but

significant increase in survival with axitinib and anti-CTLA-4 was observed, although no difference in tumor growth (luminescence) was detected (32).

An in vitro screen of small molecule inhibitors identified 6 compounds, including axitinib, that synergize with oncolytic myxoma virus against brain tumor-initiating cells (49). Here, we show that axitinib shuts down PDGFR signaling pathway and when combined with oHSV-IL12 leads to effective inactivation of the downstream oncogenic effector molecule, ERK1/2, both *in vitro* and *in vivo*. Similar to our findings, axitinib has been shown to specifically block ERK1/2 phosphorylation in patient-derived myxoid liposarcoma cell lines (50).

In conclusion, we show for the first time the combinatorial effects of axtinib+G47Δ-mIL12 in two orthotopic GSC-derived GBM models. In the human GSC immune-deficient model, we demonstrate dose-dependent anti-angiogenic effects of axitinib, with large vascularity decreases correlating with prolonged survival after combination treatment. In contrast, the anti-tumor effects of axtinib+G47Δ-mIL12 in the mouse immune-competent GBM model were mainly T cell dependent. Both mechanisms are important in that some GBM patients are on immunosuppressive doses of corticosteroids and chemotherapy and others are not.

Supplementary Material

Refer to Web version on PubMed Central for supplementary material.

Acknowledgments

Grant Support: Funded in part by grants from NIH (R01NS032677 to RLM and R01CA160762 to SDR) and The Thomas A. Pappas Chair in Neurosciences (SDR).

We thank Dr. I. Verma (Salk Institute, San Diego CA) for providing the 005 GSCs and Pfizer for providing axitinib. We thank M. Humphrey for assistance with surgeries, Camille Cushman for assistance with IHC, and animal facility personnel for taking care of animals.

References

1. Delgado-Lopez PD, Corrales-Garcia EM. Survival in glioblastoma: a review on the impact of treatment modalities. Clin Transl Oncol. 2016; 18(11):1062–71. DOI: 10.1007/s12094-016-1497-x [PubMed: 26960561]
2. Dirks PB. Brain tumor stem cells: the cancer stem cell hypothesis writ large. Mol Oncol. 2010; 4(5): 420–30. DOI: 10.1016/j.molonc.2010.08.001 [PubMed: 20801091]
3. Wakimoto H, Mohapatra G, Kanai R, Curry WT Jr, Yip S, Nitta M, et al. Maintenance of primary tumor phenotype and genotype in glioblastoma stem cells. Neuro Oncol. 2012; 14(2):132–44. DOI: 10.1093/neuonc/nor195 [PubMed: 22067563]
4. Auffinger B, Spencer D, Pytel P, Ahmed AU, Lesniak MS. The role of glioma stem cells in chemotherapy resistance and glioblastoma multiforme recurrence. Expert Rev Neurother. 2015; 15(7):741–52. DOI: 10.1586/14737175.2015.1051968 [PubMed: 26027432]
5. Lathia JD, Mack SC, Mulkearns-Hubert EE, Valentim CL, Rich JN. Cancer stem cells in glioblastoma. Genes Dev. 2015; 29(12):1203–17. DOI: 10.1101/gad.261982.115 [PubMed: 26109046]
6. Das S, Marsden PA. Angiogenesis in glioblastoma. N Engl J Med. 2013; 369(16):1561–3. DOI: 10.1056/NEJMcibr1309402 [PubMed: 24131182]
7. Jain RK, di Tomaso E, Duda DG, Loeffler JS, Sorensen AG, Batchelor TT. Angiogenesis in brain tumours. Nat Rev Neurosci. 2007; 8(8):610–22. DOI: 10.1038/nrn2175 [PubMed: 17643088]

8. Hardee ME, Zagzag D. Mechanisms of glioma-associated neovascularization. Am J Pathol. 2012; 181(4):1126–41. DOI: 10.1016/j.ajpath.2012.06.030 [PubMed: 22858156]

9. Gatson NN, Chiocca EA, Kaur B. Anti-angiogenic gene therapy in the treatment of malignant gliomas. Neurosci Lett. 2012; 527(2):62–70. DOI: 10.1016/j.neulet.2012.08.001 [PubMed: 22906922]

10. Batchelor TT, Reardon DA, de Groot JF, Wick W, Weller M. Antiangiogenic therapy for glioblastoma: current status and future prospects. Clin Cancer Res. 2014; 20(22):5612–9. DOI: 10.1158/1078-0432.CCR-14-0834 [PubMed: 25398844]

11. Wick W, Chinot OL, Bendszus M, Mason W, Henriksson R, Saran F, et al. Evaluation of pseudoprogression rates and tumor progression patterns in a phase III trial of bevacizumab plus radiotherapy/temozolomide for newly diagnosed glioblastoma. Neuro Oncol. 2016; 18(10):1434–41. DOI: 10.1093/neuonc/now091 [PubMed: 27515827]

12. Lombardi G, Pambuku A, Bellu L, Farina M, Della Puppa A, Denaro L, et al. Effectiveness of antiangiogenic drugs in glioblastoma patients: A systematic review and meta-analysis of randomized clinical trials. Crit Rev Oncol Hematol. 2017; 111:94–102. DOI: 10.1016/j.critrevonc.2017.01.018 [PubMed: 28259301]

13. Nigim F, Cavanaugh J, Patel AP, Curry WT Jr, Esaki S, Kasper EM, et al. Targeting Hypoxia-Inducible Factor 1alpha in a New Orthotopic Model of Glioblastoma Recapitulating the Hypoxic Tumor Microenvironment. J Neuropathol Exp Neurol. 2015; 74(7):710–22. DOI: 10.1097/NEN.0000000000000210 [PubMed: 26083570]

14. Cheema TA, Wakimoto H, Fecci PE, Ning J, Kuroda T, Jeyaretna DS, et al. Multifaceted oncolytic virus therapy for glioblastoma in an immunocompetent cancer stem cell model. Proc Natl Acad Sci U S A. 2013; 110(29):12006–11. DOI: 10.1073/pnas.1307935110 [PubMed: 23754388]

15. Marumoto T, Tashiro A, Friedmann-Morvinski D, Scadeng M, Soda Y, Gage FH, et al. Development of a novel mouse glioma model using lentiviral vectors. Nat Med. 2009; 15(1):110–6. DOI: 10.1038/nm.1863 [PubMed: 19122659]

16. Russell SJ, Peng KW, Bell JC. Oncolytic virotherapy. Nat Biotechnol. 2012; 30(7):658–70. DOI: 10.1038/nbt.2287 [PubMed: 22781695]

17. Saha D, Ahmed SS, Rabkin SD. Exploring the Antitumor Effect of Virus in Malignant Glioma. Drugs Future. 2015; 40(11):739–49. DOI: 10.1358/dof.2015.040.11.2383070 [PubMed: 26855472]

18. Peters C, Rabkin SD. Designing Herpes Viruses as Oncolytics. Mol Ther Oncolytics. 2015; 2doi: 10.1038/mto.2015.10

19. Saha D, Wakimoto H, Rabkin SD. Oncolytic herpes simplex virus interactions with the host immune system. Curr Opin Virol. 2016; 21:26–34. DOI: 10.1016/j.coviro.2016.07.007 [PubMed: 27497296]

20. Kohlhapp FJ, Kaufman HL. Molecular Pathways: Mechanism of Action for Talimogene Laherparepvec, a New Oncolytic Virus Immunotherapy. Clin Cancer Res. 2016; 22(5):1048–54. DOI: 10.1158/1078-0432.CCR-15-2667 [PubMed: 26719429]

21. Todo T, Martuza RL, Rabkin SD, Johnson PA. Oncolytic herpes simplex virus vector with enhanced MHC class I presentation and tumor cell killing. Proc Natl Acad Sci U S A. 2001; 98(11):6396–401. DOI: 10.1073/pnas.101136398 [PubMed: 11353831]

22. Fukuhara H, Ino Y, Todo T. Oncolytic virus therapy: A new era of cancer treatment at dawn. Cancer Sci. 2016; 107(10):1373–9. DOI: 10.1111/cas.13027 [PubMed: 27486853]

23. Zhang W, Fulci G, Wakimoto H, Cheema TA, Buhrman JS, Jeyaretna DS, et al. Combination of oncolytic herpes simplex viruses armed with angiostatin and IL-12 enhances antitumor efficacy in human glioblastoma models. Neoplasia. 2013; 15(6):591–9. [PubMed: 23730207]

24. Hu-Lowe DD, Zou HY, Grazzini ML, Hallin ME, Wickman GR, Amundson K, et al. Nonclinical antiangiogenesis and antitumor activities of axitinib (AG-013736), an oral, potent, and selective inhibitor of vascular endothelial growth factor receptor tyrosine kinases 1, 2, 3. Clin Cancer Res. 2008; 14(22):7272–83. DOI: 10.1158/1078-0432.CCR-08-0652 [PubMed: 19010843]

25. Motzer RJ, Escudier B, Tomczak P, Hutson TE, Michaelson MD, Negrier S, et al. Axitinib versus sorafenib as second-line treatment for advanced renal cell carcinoma: overall survival analysis and

updated results from a randomised phase 3 trial. Lancet Oncol. 2013; 14(6):552–62. DOI: 10.1016/S1470-2045(13)70093-7 [PubMed: 23598172]

26. Schiller JH, Larson T, Ou SH, Limentani S, Sandler A, Vokes E, et al. Efficacy and safety of axitinib in patients with advanced non-small-cell lung cancer: results from a phase II study. J Clin Oncol. 2009; 27(23):3836–41. DOI: 10.1200/JCO.2008.20.8355 [PubMed: 19597027]
27. McNamara MG, Le LW, Horgan AM, Aspinall A, Burak KW, Dhani N, et al. A phase II trial of second-line axitinib following prior antiangiogenic therapy in advanced hepatocellular carcinoma. Cancer. 2015; 121(10):1620–7. DOI: 10.1002/cncr.29227 [PubMed: 25565269]
28. Ho AL, Dunn L, Sherman EJ, Fury MG, Baxi SS, Chandramohan R, et al. A phase II study of axitinib (AG-013736) in patients with incurable adenoid cystic carcinoma. Ann Oncol. 2016; 27(10):1902–8. DOI: 10.1093/annonc/mdw287 [PubMed: 27566443]
29. Duerinck J, Du Four S, Vandervorst F, D'Haene N, Le Mercier M, Michotte A, et al. Randomized phase II study of axitinib versus physicians best alternative choice of therapy in patients with recurrent glioblastoma. J Neurooncol. 2016; 128(1):147–55. DOI: 10.1007/s11060-016-2092-2 [PubMed: 26935577]
30. Lu L, Saha D, Martuza RL, Rabkin SD, Wakimoto H. Single agent efficacy of the VEGFR kinase inhibitor axitinib in preclinical models of glioblastoma. J Neurooncol. 2015; 121(1):91–100. DOI: 10.1007/s11060-014-1612-1 [PubMed: 25213669]
31. Du Four S, Maenhout SK, De Pierre K, Renmans D, Niclou SP, Thielemans K, et al. Axitinib increases the infiltration of immune cells and reduces the suppressive capacity of monocytic MDSCs in an intracranial mouse melanoma model. Oncoimmunology. 2015; 4(4):e998107.doi: 10.1080/2162402X.2014.998107 [PubMed: 26137411]
32. Du Four S, Maenhout SK, Benteyn D, De Keersmaecker B, Duerinck J, Thielemans K, et al. Disease progression in recurrent glioblastoma patients treated with the VEGFR inhibitor axitinib is associated with increased regulatory T cell numbers and T cell exhaustion. Cancer Immunol Immunother. 2016; 65(6):727–40. DOI: 10.1007/s00262-016-1836-3 [PubMed: 27098427]
33. Saha D, Martuza RL, Rabkin SD. Macrophage Polarization Contributes to Glioblastoma Eradication by Combination Immunovirotherapy and Immune Checkpoint Blockade. Cancer Cell. 2017; 32(2):253–67. e5. DOI: 10.1016/j.ccell.2017.07.006 [PubMed: 28810147]
34. Wakimoto H, Kesari S, Farrell CJ, Curry WT Jr, Zaupa C, Aghi M, et al. Human glioblastoma-derived cancer stem cells: establishment of invasive glioma models and treatment with oncolytic herpes simplex virus vectors. Cancer Res. 2009; 69(8):3472–81. DOI: 10.1158/0008-5472.CAN-08-3886 [PubMed: 19351838]
35. Hu Y, Smyth GK. ELDA: extreme limiting dilution analysis for comparing depleted and enriched populations in stem cell and other assays. J Immunol Methods. 2009; 347(1–2):70–8. DOI: 10.1016/j.jim.2009.06.008 [PubMed: 19567251]
36. Kanai R, Wakimoto H, Martuza RL, Rabkin SD. A novel oncolytic herpes simplex virus that synergizes with phosphoinositide 3-kinase/Akt pathway inhibitors to target glioblastoma stem cells. Clin Cancer Res. 2011; 17(11):3686–96. DOI: 10.1158/1078-0432.CCR-10-3142 [PubMed: 21505062]
37. Chen G, Gulbranson DR, Yu P, Hou Z, Thomson JA. Thermal stability of fibroblast growth factor protein is a determinant factor in regulating self-renewal, differentiation, and reprogramming in human pluripotent stem cells. Stem Cells. 2012; 30(4):623–30. DOI: 10.1002/stem.1021 [PubMed: 22213113]
38. WuDunn D, Spear PG. Initial interaction of herpes simplex virus with cells is binding to heparan sulfate. J Virol. 1989; 63(1):52–8. [PubMed: 2535752]
39. Stehle F, Schulz K, Fahldieck C, Kalich J, Lichtenfels R, Riemann D, et al. Reduced immunosuppressive properties of axitinib in comparison with other tyrosine kinase inhibitors. J Biol Chem. 2013; 288(23):16334–47. DOI: 10.1074/jbc.M112.437962 [PubMed: 23625925]
40. Postow MA, Chesney J, Pavlick AC, Robert C, Grossmann K, McDermott D, et al. Nivolumab and ipilimumab versus ipilimumab in untreated melanoma. N Engl J Med. 2015; 372(21):2006–17. DOI: 10.1056/NEJMoa1414428 [PubMed: 25891304]
41. Morelli MB, Amantini C, Nabissi M, Cardinali C, Santoni M, Bernardini G, et al. Axitinib induces senescence-associated cell death and necrosis in glioma cell lines: The proteasome inhibitor,

bortezomib, potentiates axitinib-induced cytotoxicity in a p21(Waf/Cip1) dependent manner. Oncotarget. 2017; 8(2):3380–95. DOI: 10.18632/oncotarget.13769 [PubMed: 27926485]

42. Ning J, Wakimoto H, Peters C, Martuza RL, Rabkin SD. Rad51 Degradation: Role in Oncolytic Virus-Poly(ADP-Ribose) Polymerase Inhibitor Combination Therapy in Glioblastoma. J Natl Cancer Inst. 2017; 109(3):1–13. DOI: 10.1093/jnci/djw229
43. Huang Y, Yuan J, Righi E, Kamoun WS, Ancukiewicz M, Nezivar J, et al. Vascular normalizing doses of antiangiogenic treatment reprogram the immunosuppressive tumor microenvironment and enhance immunotherapy. Proc Natl Acad Sci U S A. 2012; 109(43):17561–6. DOI: 10.1073/pnas.1215397109 [PubMed: 23045683]
44. Ornstein MC, Wood L, Elson P, Allman K, Beach J, Martin A, et al. Clinical Effect of Dose Escalation After Disease Progression in Patients With Metastatic Renal Cell Carcinoma. Clin Genitourin Cancer. 2017; 15(2):e275–e80. DOI: 10.1016/j.clgc.2016.08.014 [PubMed: 27625016]
45. Kwilas AR, Ardiani A, Donahue RN, Aftab DT, Hodge JW. Dual effects of a targeted small-molecule inhibitor (cabozantinib) on immune-mediated killing of tumor cells and immune tumor microenvironment permissiveness when combined with a cancer vaccine. J Transl Med. 2014; 12:294.doi: 10.1186/s12967-014-0294-y [PubMed: 25388653]
46. Bose A, Lowe DB, Rao A, Storkus WJ. Combined vaccine+axitinib therapy yields superior antitumor efficacy in a murine melanoma model. Melanoma Res. 2012; 22(3):236–43. DOI: 10.1097/CMR.0b013e3283538293 [PubMed: 22504156]
47. Garber K. Promising early results for immunotherapy-antiangiogenesis combination. J Natl Cancer Inst. 2014; 106(11)doi: 10.1093/jnci/dju392
48. Wilmes LJ, Pallavicini MG, Fleming LM, Gibbs J, Wang D, Li KL, et al. AG-013736, a novel inhibitor of VEGF receptor tyrosine kinases, inhibits breast cancer growth and decreases vascular permeability as detected by dynamic contrast-enhanced magnetic resonance imaging. Magn Reson Imaging. 2007; 25(3):319–27. DOI: 10.1016/j.mri.2006.09.041 [PubMed: 17371720]
49. McKenzie BA, Zemp FJ, Pisklakova A, Narendran A, McFadden G, Lun X, et al. In vitro screen of a small molecule inhibitor drug library identifies multiple compounds that synergize with oncolytic myxoma virus against human brain tumor-initiating cells. Neuro Oncol. 2015; 17(8):1086–94. DOI: 10.1093/neuonc/nou359 [PubMed: 25605818]
50. Kerr LT, Donoghue JF, Wilding AL, Johns TG. Axitinib Has Antiangiogenic and Antitumorigenic Activity in Myxoid Liposarcoma. Sarcoma. 2016; 2016:3484673.doi: 10.1155/2016/3484673 [PubMed: 27822137]

TRANSLATIONAL RELEVANCE

Glioblastoma (GBM) is a lethal brain tumor containing a subpopulation of GBM stem-like cells (GSCs), thought to initiate tumorigenesis and contribute to therapy resistance. GBM is a complex malignancy consisting of neoplastic cells, including GSCs and bulk tumor cells, and non-neoplastic cells, including innate and adaptive immune cells and dysregulated vasculature. Targeting these different components will likely be necessary to treat GBM. Therefore, we combined oncolytic herpes simplex virus (oHSV) that selectively kills cancer cells with VEFGR tyrosine kinase inhibitor axitinib in 2 aggressive GSC-derived orthotopic tumor models: patient-derived MGG123 in immune-deficient mice and syngeneic 005 in immune-competent mice. This combination significantly prolonged survival in both models and involved multiple activities: direct oncolysis, increased macrophage infiltration, anti-angiogenesis and PDGFR/ERK pathway inhibition in MGG123, and T-cell-dependent activity in 005. Since axitinib and oHSV are already in clinical trials for GBM as monotherapy with limited efficacy, this strategy is of translational relevance.

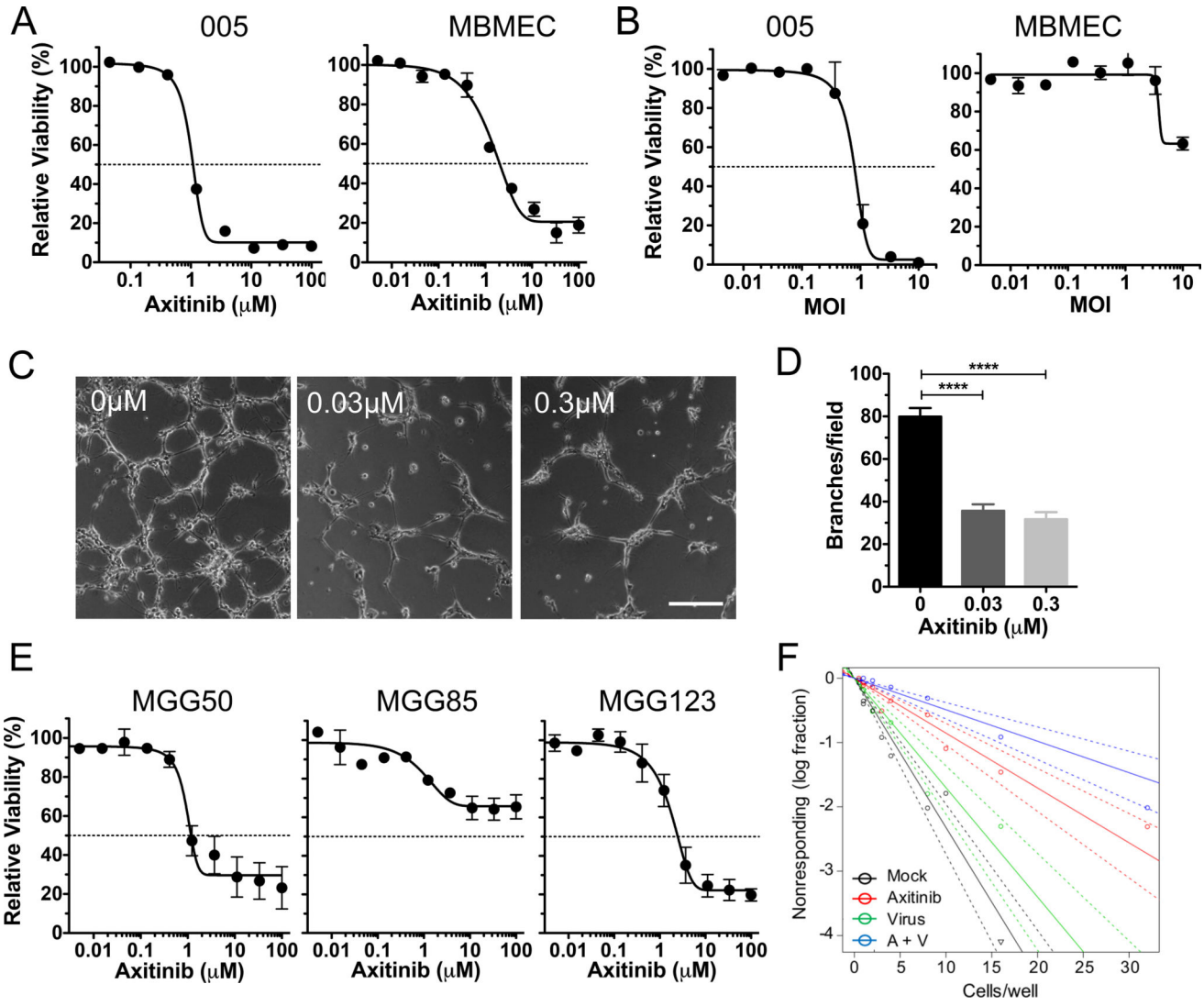

Figure 1. Cytotoxic effects of axitinib and G47Δ-mIL12 in mouse and human cells *in vitro*

A, B. Dose response curves for axitinib (**A**) and G47Δ-mIL12 (**B**) in 005 GSCs after 4 days and MBMEC after 5 days; each graph represents an average of 2–4 experiments performed in triplicate. For G47Δ-mIL12 experiments (**B**), cells were seeded in their respective media with 'no heparin', virus was added 0 hr (for MBMEC) or 5 hr (for 005) post-seeding, and viability measured by MTS assay. **C, D.** Axitinib reduced matrigel-based tube formation in 005 GSCs. **C.** Microscopic images of representative wells imaged at 20× are shown. Bar = 100 μm. **D**. Quantification of branching point counts from 3–5 random fields/well. The numbers of tube branches were significantly reduced after axitinib treatment (0.03μM or 0.3μM) compared to mock treatment. Experiment was performed in triplicate. Tukey's multiple comparison test was used to compare the different treatment groups; ****$P <$ 0.0001. **E**. Cytotoxic effects of axitinib in human GSCs *in vitro*. Dose response curves for axitinib in MGG50, MGG85, and MGG123 GSCs after 6 days, as measured by MTS assay; each graph represents an average of three experiments performed in triplicate. **F**. *In vitro* limiting dilution study. 005 cells were plated in 96-well plate. Cells were continuously

exposed to a non-toxic concentration of axitinib (300 nM) and/or G47Δ-mIL12 (moi 0.1) for 12 days and number of wells (n=30 wells total) containing spheres were recorded and plotted using ELDA: Extreme Limiting Dilution Analysis form, as described (35). Estimated stem cell frequencies were; 1 in 4.3 for mock, 1 in 11.7 for axitinib, 1 in 5.9 for virus, and 1 in 20.4 for combination. Treatment groups were compared to each other using a Chi Square test: mock vs. axitinib, $p=7.9 \times 10^{-15}$; mock vs. virus, p=0.024; mock vs. combination, $p=1,1 \times 10^{-25}$; axitinib vs. virus, $p=5.1 \times 10^{-6}$; axitinib vs. combination, p=0.0006; virus vs. combination, $p=5.6 \times 10^{-13}$.

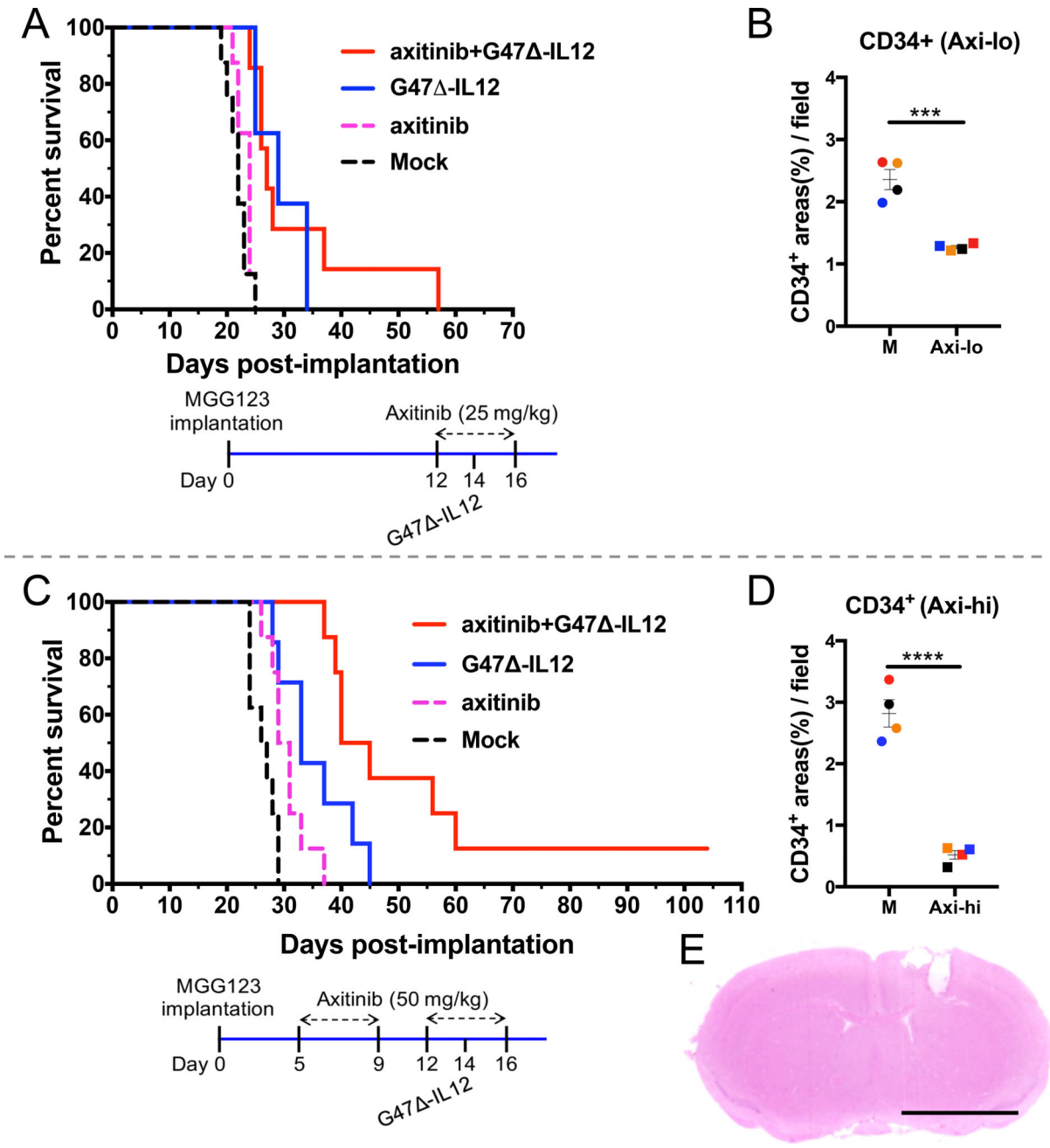

Figure 2. Axitinib treatment in combination with intratumoral G47Δ-mIL12 in athymic mice bearing human MGG123 GSC-derived brain tumors

A. Kaplan-Meier survival curve. Athymic mice were implanted with MGG123 human GSCs on day 0, axitinib (25 mg/kg) or vehicle solution was injected intraperitoneally from days 12 to 16, and/or G47Δ-mIL12 (5×10^4 pfu) or PBS injected intratumorally on day 14. n=8, except for combination, n=7. Mock vs. axitinib, p=0.16; mock vs. G47Δ-mIL12, p=0.0003; mock vs. combination, p=0.0003; axitinib vs. combination, p=0.0008; G47Δ-mIL12 vs. combination, p=0.78. **B.** Immunohistochemical staining of $CD34^+$ endothelial cells in brain tumor sections from mice treated with low-dose axitinib (25 mg/kg). Athymic nude mice implanted with MGG123 GSCs (5×10^4) on day 0 and treated with axitinib (25 mg/kg) or

vehicle solution following the schema shown in A. Twenty-four hours after the last axitinib injection (day 17), animals were sacrificed and brains collected. Formalin-fixed and paraffin-embedded brain tumor sections were stained for $CD34^+$ endothelial cells. Scatter plot (each animal 1 point) showing the quantification of $CD34^+$ areas (10× objective) from 5 fields / tumor section (2 sections / mouse; n=4 mice/group). Quantification of $CD34^+$ areas was done by ImageJ software (NIH). Counter was blinded to the experiment. **C.** Kaplan-Meier survival curve. Athymic mice were implanted with MGG123 human GSCs and treated with G47Δ-mIL12 or PBS intratumorally on day 14 (as in A). High dosage of axitinib (50 mg/kg) or vehicle solution was administered intraperitoneally from days 5 to 16 (2 cycles of 5 days on and 2 days off). n=8, except for G47Δ-mIL12, n=7. The long-term surviving mouse from the combination group was sacrificed on day 104, and tumor was not present, shown in E. Mock vs. axitinib, p=0.009; mock vs. G47Δ-mIL12, p=0.002; mock vs. combination, p=<0.0001; axitinib vs. G47Δ-mIL12, p=0.08; axitinib vs. combination, p=<0.0001; G47Δ-mIL12 vs. combination, p=0.02. **D.** Immunohistochemical staining of $CD34^+$ endothelial cells in brain tumor sections from mice treated with high-dose axitinib (50 mg/kg). Same data as in Fig. 3B. Mean ± SEM. *** P<0.001, **** P<0.0001. **E.** Hematoxylin and eosin staining of brain section of long-term survivor mouse in C. Mouse was sacrificed on day 104 and H&E stained brain section showing the needle track wound (right hemisphere) with no evidence of tumor. Bar = 0.1 inch.

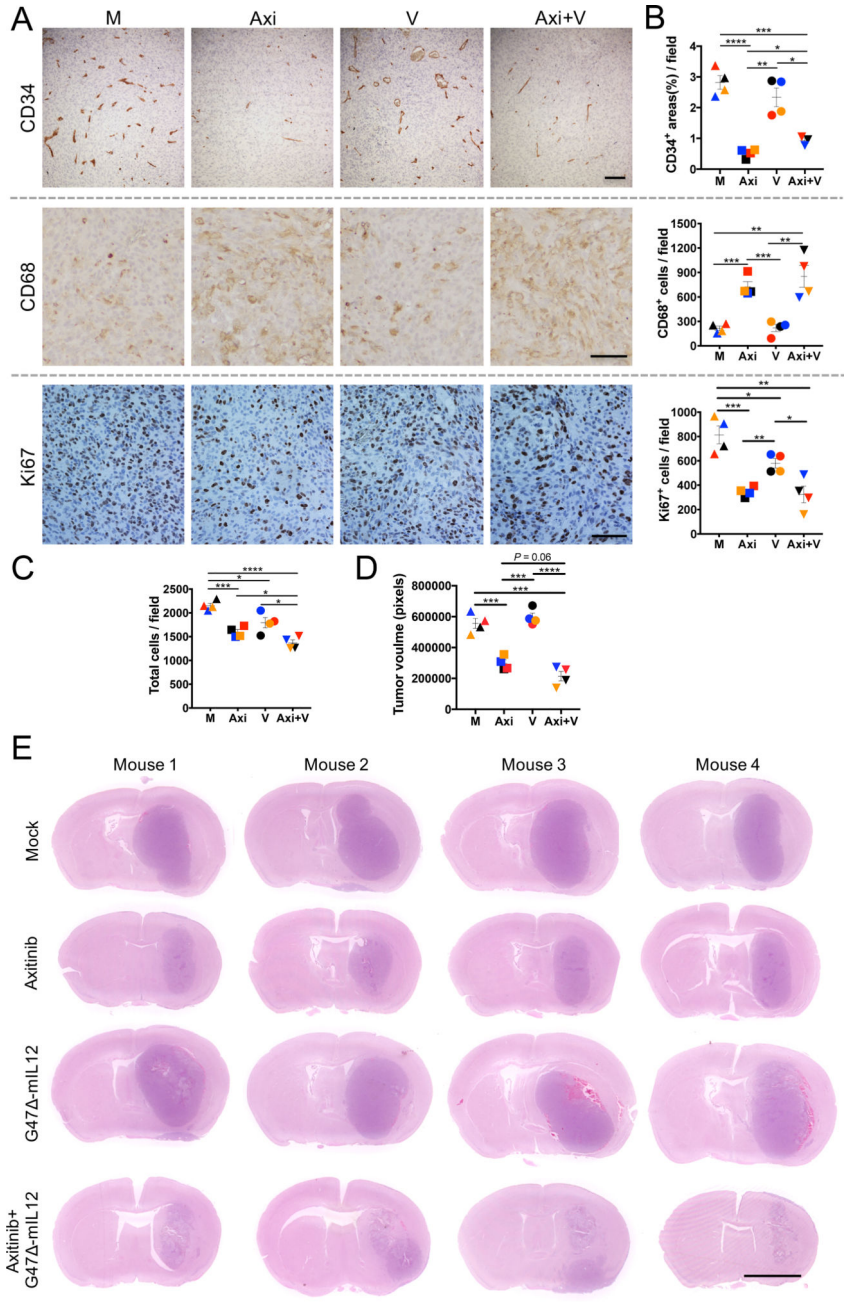

Figure 3. Histopathological analyses of therapeutic effects in the MGG123 GSC-derived brain tumor model

Athymic mice were implanted with MGG123 GSCs (5×10^4) on day 0. Axitinib (50 mg/kg) or vehicle solution was injected intraperitoneally from days 5 to 16 (2 cycles of 5 days on and 2 days off) and G47Δ-mIL12 (5×10^4 pfu) or PBS injected intratumorally on day 14. Twenty-four hours after the last axitinib injection mice were sacrificed and brains collected. Formalin-fixed and paraffin-embedded brain tumor sections were stained for CD34, CD68 and Ki67. **A**. Representative images from sections with immunohistochemical staining for CD34 (upper), CD68 (middle), and Ki67 (lower). Brown indicates positivity. Bars = 100 μm. **B**. Scatter plot (each animal 1 point) of the quantification of $CD34^+$ areas (10× objective),

$CD68^+$ cells (20× objective), and $Ki67^+$ cells (20× objective) from 3 fields / tumor section (1 section / mouse for CD34 and Ki67 and 2 sections / mouse for CD68). **C**. Scatter plot (each animal 1 point) of the quantification of total cells within the tumor mass, using sections stained for Ki67 and counter-stained with hematoxylin. **D.** Quantification of tumor volume using images shown in E. Individual mice in each group (mock, M; axitinib, Axi; G47Δ-mIL12, V; and axitinib+ G47Δ-mIL12, Axi+V) identified by color. **E.** Hematoxylin and eosin staining of brain tumor sections. Scanned images of mouse brain sections from mice bearing MGG123 GSC-derived GBM tumors. Bars = 0.1 inch. Mean ± SEM. * $P<0.05$, ** $P<0.01$, *** $P<0.001$, **** $P<0.0001$.

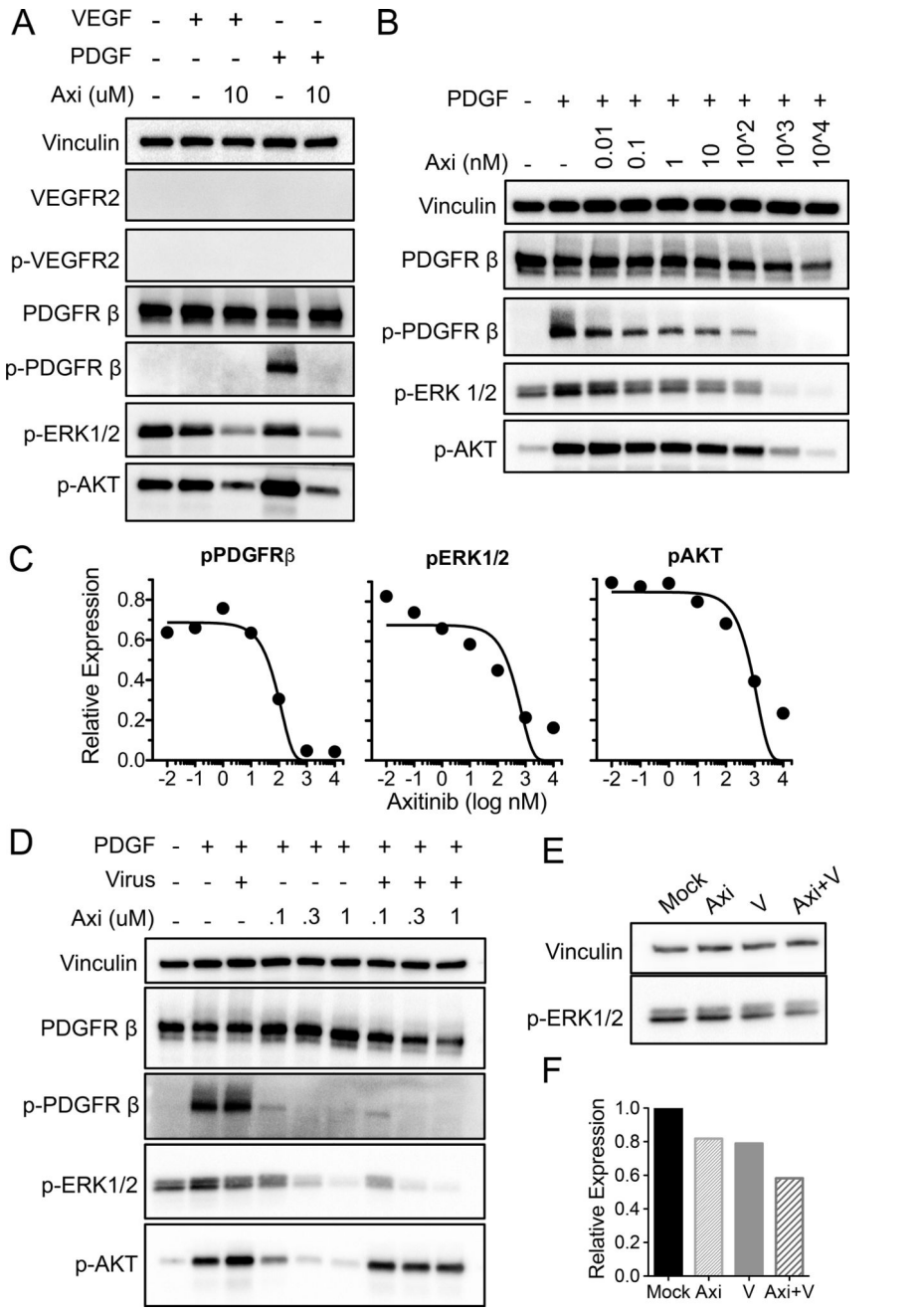

Figure 4. Effects of axitinib and/or G47Δ-mIL12 on VEGFR and PDGFR signaling pathways in MGG123 GBM

A. Effects of axitinib on VEGFR and PDGFR signaling pathway in MGG123 GSCs *in vitro*. Cells were starved (no growth factors) overnight, followed by stimulation with or without recombinant human VEGF (100 ng/ml) or PDGF (100 ng/ml) for 15 min. Simultaneously, cells were also treated with or without axitinib (10 μM) for 15 min. Cell lysates were processed for western blotting with antibodies to Vinculin, VEGFR2, p-VEGFR2, PDGFRβ, p-PDGFRβ, p-ERK1/2, and p-AKT (Cell Signaling). **B.** Representative blot of dose-dependent effects of axitinib (dose indicated) on PDGFRβ signaling. **C.** Relative expression (to vinculin; mean) of p-PDGFRβ, p-ERK1/2, and p-AKT obtained from B and second blot.

Lines are curve fit of data (nonlinear regression, Gaussian distribution). **D.** Representative blot of effects of combination (axitinib+G47Δ-mIL12) treatment on PDGFRβ signaling. Starved MGG123 cells were inoculated with G47Δ-mIL12 (moi 1.0) and incubated for 6 hr at 37°C. During the last 15 min of viral incubation, PDGF (100 ng/ml) and axitinib (111, 333, or 1000 nM) were added to the cells. Cells were then processed for western blotting. Quantification in Supplementary Fig. S5C. **E.** Treatment effects of combination therapy (axitinib+G47Δ-mIL12) on p-ERK1/2 in MGG123 tumors *in vivo*. Athymic mice were implanted with MGG123 human GSCs on day 0, high-dose axitinib (50 mg/kg) or vehicle solution was injected intraperitoneally from days 13–17, and/or G47Δ-mIL12 (5×10^4 pfu) or PBS injected intratumorally on day 15, and 3 hr after the last axitinib injection (i.e., day 17), mice were sacrificed (3–4 mice/group) and brain tumor quadrants were collected. Tumor quadrants from each group were pooled and processed for western blotting with antibodies to p-ERK1/2 and vinculin. **F.** Relative expression (to vinculin) of p-ERK1/2 obtained from E.

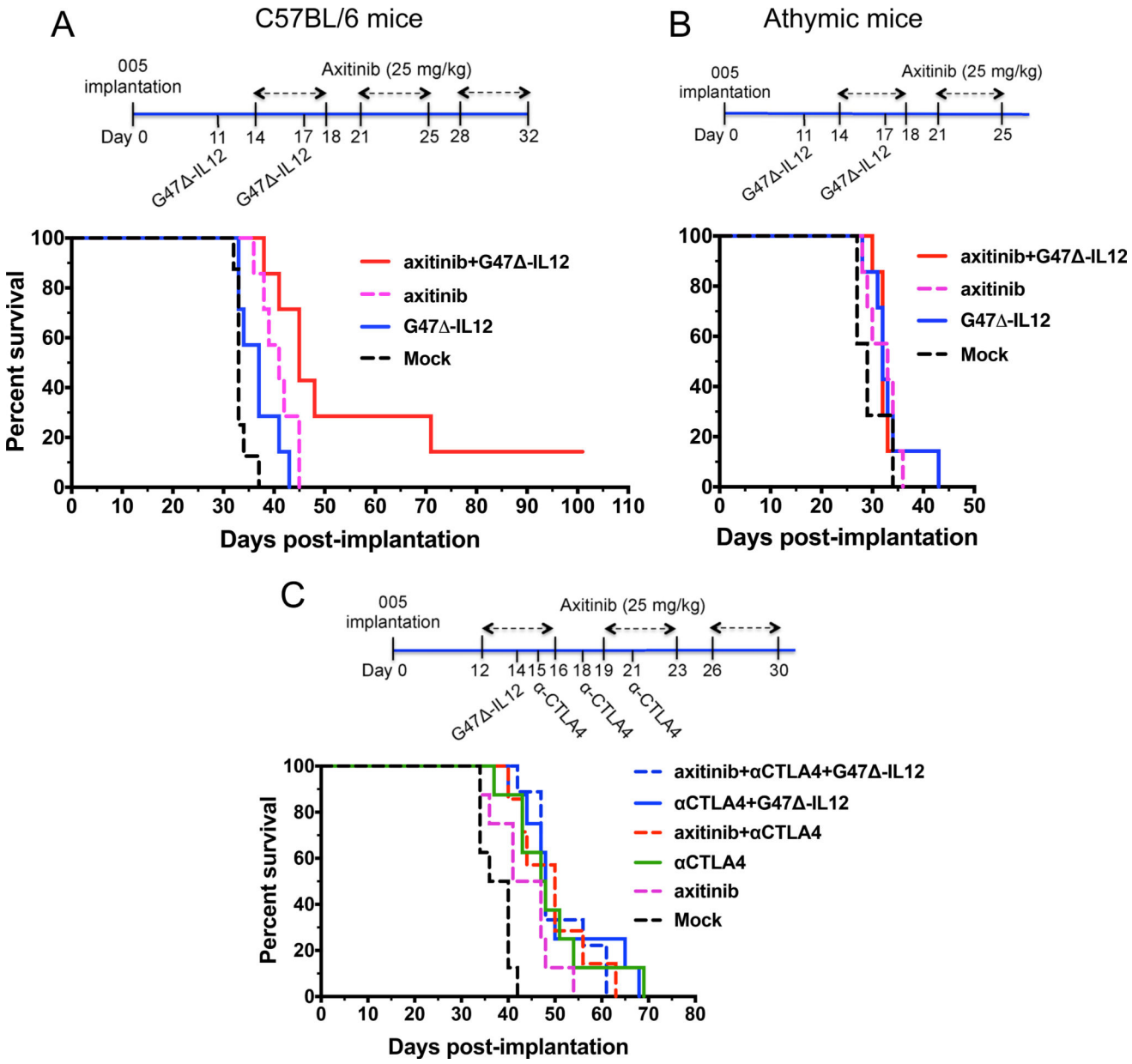

Figure 5. A, B. Effects of combination therapy (axitinib+G47Δ-mIL12) in orthotopic 005 GSC-derived GBM model in immune-competent and immune-compromised settings

A. Systemic TKI axitinib, intratumoral G47Δ-mIL12, or the combination prolongs survival in C57Bl/6 mice. C57Bl/6 mice implanted with 005 GSCs were treated with G47Δ-mIL12 (1×10^5 pfu) or PBS injected intratumorally on days 11 and 17 and/or axitinib (25 mg/kg) or vehicle solution injected intraperitoneally from days 14 to 32 (3 cycles of 5 days on and 2 days off) (n=7/group, except Mock, n=8). The long-term surviving mouse from the combination group was sacrificed on day 101, and a large tumor was present (Supplementary Fig. S6A). Mock vs. axitinib, p=0.0003; mock vs. G47Δ-mIL12, p=0.03; mock vs. combination, p=<0.0001; axitinib vs. G47Δ-mIL12, p=0.09; axitinib vs. combination, p=0.04; G47Δ-mIL12 vs. combination, p=0.002. **B.** Systemic TKI axitinib, intratumoral G47Δ-mIL12, or the combination does not produce any survival benefits in

athymic mice. Athymic mice implanted with 005 GSCs were treated with G47Δ-mIL12 (1×10^5 pfu) or PBS injected intratumorally on days 11 and 17 and/or axitinib (25 mg/kg) or vehicle injected intraperitoneally from days 14 to 25 (2 cycles of 5 days on and 2 days off) (n=7/group). No significant differences were observed between combination and single treatments or compared with mock (p=>0.05). **C. Systemic immune checkpoint inhibitor does not produce any survival advantage when added in combination with axitinib +G47Δ-mIL12 therapy for the treatment of 005 GSC-derived brain tumors**. C57Bl/6 mice were implanted with 005 GSCs (2×10^4) on day 0. Axitinib (25 mg/kg) or vehicle injected intraperitoneally from days 12 to 30 (3 cycles of 5 days on and 2 days off). G47Δ-mIL12 (2.5×10^5 pfu) or PBS was injected intratumorally on day 14 and anti-CTLA-4 antibody (5 mg/kg), or isotype control IgG (5 mg/kg) intraperitoneally on days 15, 18 and 21. Median survival of Mock (38 days; n=8) was significantly different (p<0.05) from all treatments groups: axitinib (44 days; n=8), anti-CTLA-4 (47.5 days; n=8), axitinib+anti-CTLA-4 (50 days; n=7), anti-CTLA-4+G47Δ-mIL12 (48 days; n=8), or axitinib+anti-CTLA-4+G47Δ-mIL12 (48 days; n=9). No significant difference was observed between the single and dual or triple combination treatments (p=>0.05).

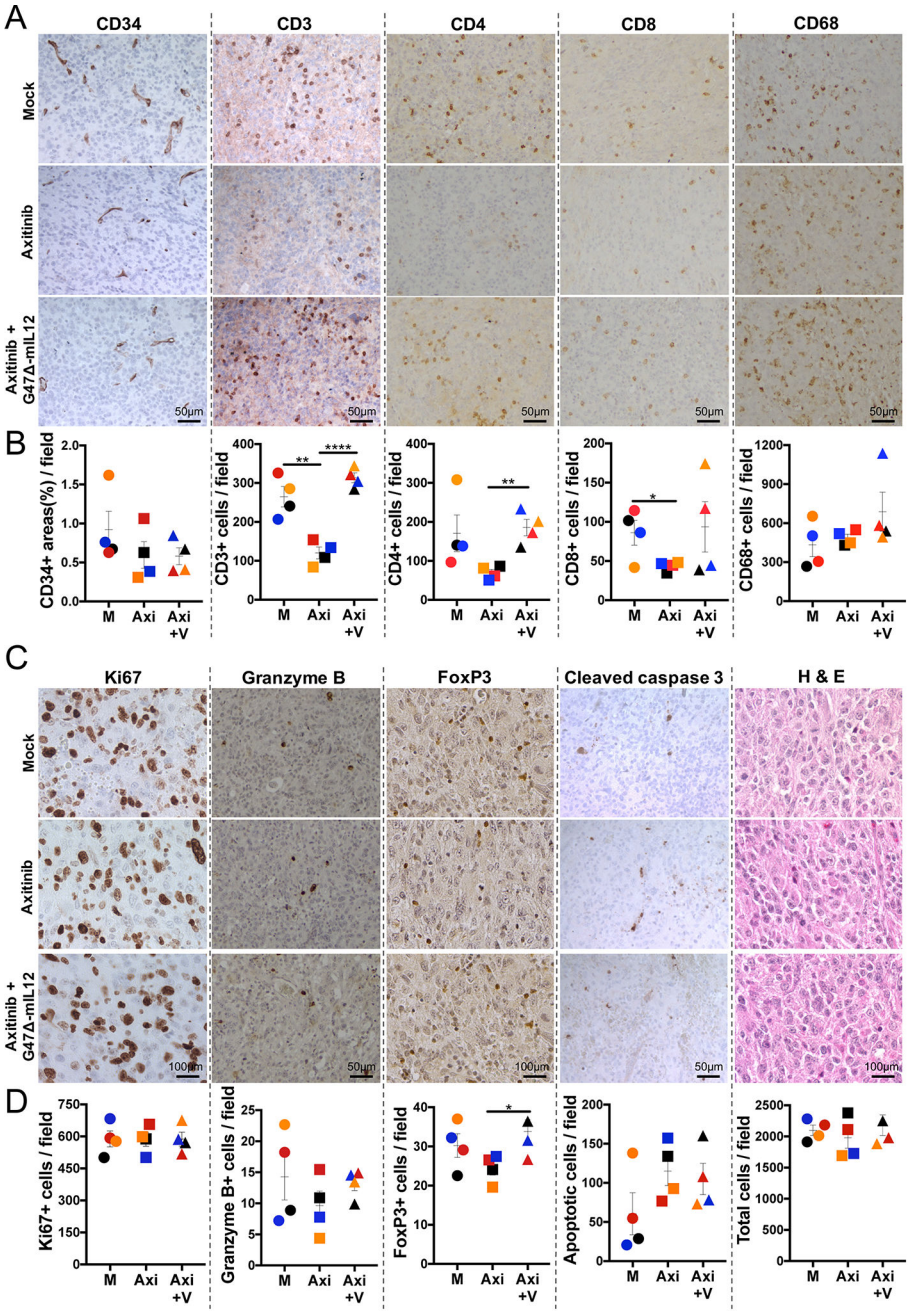

Figure 6. Immunohistochemical staining of cell markers in brain tumor sections

C57Bl/6 mice implanted with 005 GSCs (2×10^4) on day 0 were injected intratumorally with G47Δ-mIL12 (1×10^5 pfu) or PBS on days 18 and 24 and intraperitoneally with axitinib (25 mg/kg) or vehicle from days 21 to 25. Six hours after the last axitinib injection, animals were sacrificed and brains collected. Brain tumor sections were stained for CD34, endothelial cells; CD3, T cells; CD4, T cells; CD8, T cells; CD68, macrophages; Ki67, proliferating cells; Granzyme B, cytotoxic cells; FoxP3, regulatory T cells; cleaved caspase-3, apoptotic cells; and H & E (for total cell count). **A, C.** Representative images with positive cells stained brown. **B, D.** Scatter plots (each animal 1 point) showing the

quantification of $CD34^+$ areas (10× objective, 3 fields/tumor section, 3 sections/mouse), $CD3^+$ (10× objective, 3 fields/section, 3 sections/mouse), $CD4^+$ (10× objective, 5 fields/section, 1 section/mouse), $CD8^+$ (10× objective, 5 fields/section, 1 section/mouse), $CD68^+$ (20× objective, 5 fields/section, 1 section/mouse), $Ki67^+$ cells (20× objective, 3 fields/section, 3 sections/mouse), Granzyme B^+ (10× objective, 3 fields/section, 3 sections/mouse), $FoxP3^+$ (20× objective, 3 fields/section, 3 sections/mouse), cleaved caspase-3^+ (10× objective, 3 fields/section, 3 sections/mouse), and cell density count (20× objective, 3 fields/section, 1 section/mouse). Individual mice in each group (mock, M; axitinib, Axi; and axitinib+ G47Δ-mIL12, Axi+V) identified by color. Mean ± SEM. * $P<0.05$, ** $P<0.01$, **** $P<0.0001$. Quantification of $CD34^+$ areas was done by ImageJ software (NIH). Counter was blinded to the experiment.